

Hysteresis phenomena in $\text{Cd}_2\text{P}_2\text{S}_6$ layered crystals

Cite as: Fiz. Nizk. Temp. 51, 53–58 (January 2025); doi: 10.1063/10.0034644

Submitted: 20 November 2024



View Online



Export Citation



CrossMark

H. Ban,¹ D. Gal,² S. Motrja,¹ and A. Molnar^{1,a)}

AFFILIATIONS

¹Department of the Physics of Semiconductors, Uzhhorod National University, Uzhhorod 88000, Ukraine

²HUN-REN Wigner Research Centre for Physics, Po. Box. 49, Budapest 1525, Hungary

^{a)}Author to whom correspondence should be addressed: alex.molnar@uzhnu.edu.ua

ABSTRACT

The results of the study of the temperature dependence of the dielectric permittivity of $\text{Cd}_2\text{P}_2\text{S}_6$ crystals are presented. It is shown that in the temperature range 80–420 K there are three regions in which hysteresis phenomena are observed. At high temperatures ($T > 320$ K) there is an activation change of the dielectric losses associated with the increased conductivity of $\text{Cd}_2\text{P}_2\text{S}_6$ crystals. The transition from heating to cooling leads to a decrease in losses, which is manifested as a hysteresis in the dielectric constant. A jump-like change in dielectric permittivity is found at 228 K in the cooling mode and 265 K in the heating mode, which is due to the first-order phase transition in these crystals. The third hysteresis region appears at low temperatures of 80–90 K. When the temperature is cycled in this interval, the classical hysteresis behavior is observed with a decrease in both amplitude and temperature range with each cycle. The cause of this behavior will be the subject of further investigation.

Published under an exclusive license by AIP Publishing. <https://doi.org/10.1063/10.0034644>

1. INTRODUCTION

Single crystal cadmium hexathiohypodiphosphate, or $\text{Cd}_2\text{P}_2\text{S}_6$, also known as CdPS_3 , has attracted much attention over the past few decades due to their easy intercalation with various inorganic and organic substances.^{1,2} They are promising candidates for the creation of composite catalytic materials for hydrogenation due to their exceptional chemical and physical properties.^{3,4} $\text{Cd}_2\text{P}_2\text{S}_6$ was used as a material for a versatile superionic conductor to detect unusual nanofluidic phenomena in nanocapillaries.^{5,6} The introduction of an electrically conductive polymer into the interlayer van der Waals space of $\text{Cd}_2\text{P}_2\text{S}_6$ leads to a dramatic modification of its physical properties, which has led to various applications such as magnetic materials⁷ or nonlinear optical materials.⁸ Some elements of modern electronics have already been created based on CdPS_3 , e.g., flexible memristor for artificial synapse and logic operation.⁹

In these crystals, as shown in Ref. 10, a first-order phase transition from the high-temperature $C2/m$ phase to the low-temperature $R\bar{3}$ phase at 260 K with phase coexistence in the temperature range of 16 K is observed. Further studies (see Ref. 11) confirmed the presence of a first-order phase transition. Still, its temperature was indicated to be somewhat lower, about 228 K. Many X-ray diffraction studies^{10,11} have been conducted, which have shown that, in addition to stacking faults, the low-temperature state of CdPS_3 differs significantly from that observed at room

temperature both in the stacking mode (CdI_2 vs CdCl_2 type), on the one hand, and in the ordering of Cd atoms at octahedral noncentric positions, on the other (Fig. 1).

The structure of $\text{Cd}_2\text{P}_2\text{S}_6$ crystals can be described¹² as two-dimensional layers consisting of densely packed sulfide ions together with P_2^{8+} and Cd^{2+} ions occupying octahedral voids. In the case of $\text{Cd}_2\text{P}_2\text{S}_6$, the ABCABC stacking was found in the high-temperature monoclinic phase, and the ABAB stacking of sulfides leads to the rhombohedral structure found in the low-temperature state. The unwillingness of Cd atoms to occupy the center of the octahedral S_6 sites and their tendency to shift along the crystallographic direction c stems from the second-order Jahn-Teller effect involving the $5p$ and possibly $5s$ orbitals of Cd. The high-temperature monoclinic modification of the $\text{Cd}_2\text{P}_2\text{S}_6$ structure represents donor-acceptor interactions between the largest occupied molecular orbital and the smallest unoccupied molecular orbital $\text{P}_2\text{S}_6^{4-}$ in the neighboring layers, which are absent in the low-temperature rhombohedral phase. The off-center displacement of Cd atoms in the low-temperature phase [Fig. 1(b)] is not related to the change in the stacking order associated with the phase transition.¹²

Although a relatively large number of works have recently appeared on the synthesis and study of the physical and chemical properties of $\text{Cd}_2\text{P}_2\text{S}_6$, there is practically no data on the electro-physical properties of these crystals. Only the band gap of CdPS_3 crystals is known from Ref. 13, which is ~ 3.3 – 3.5 eV. Therefore, we

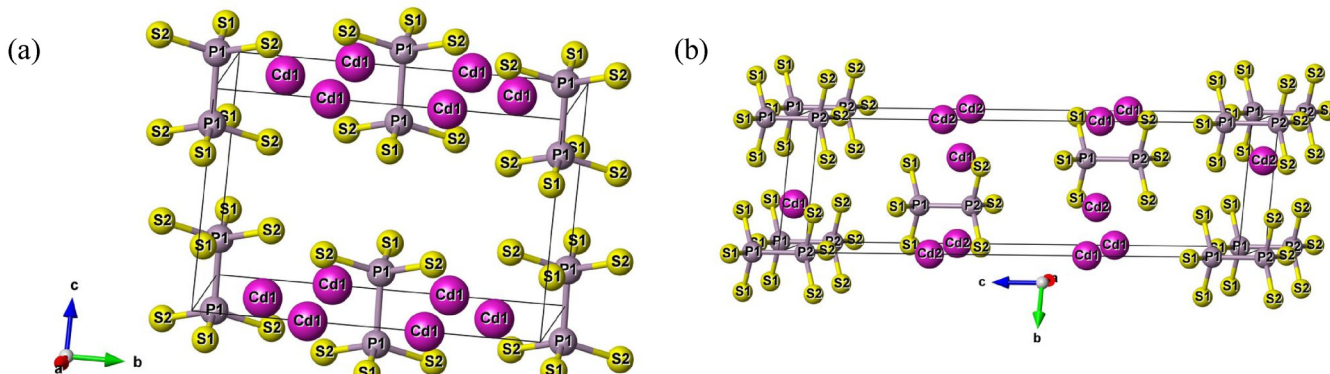


FIG. 1. The structure of $\text{Cd}_2\text{P}_2\text{S}_6$ crystals in the high-temperature phase $\text{C}2/\text{m}$ (a), and in the low-temperature phase $\text{R}3$ (b).

have studied the temperature dependence of the dielectric spectra of $\text{Cd}_2\text{P}_2\text{S}_6$ single crystals.

2. CRYSTAL GROWING

$\text{Cd}_2\text{P}_2\text{S}_6$ crystals were obtained by heating the constituent elements in stoichiometric proportions (1:1:3) in a vacuum quartz ampoule at a temperature of 983 K, which was maintained for 10 days.¹⁴ The material obtained consisted mainly of small translucent white crystals, but also included several large thin single crystals with an area of about 1 cm^2 and a thickness of 5–50 μm [see Fig. 2(a)].

Since the obtained crystals were not plane-parallel (there were growth steps on the surface), the plane-parallelism of the samples was realized by chipping the investigated crystals. The result was an almost perfectly flat surface. As we can see in Fig. 2(b), obtained by Bruker Dimension Icon AFM provided by Bruker Nano Inc., the surface irregularities are less than $\pm 15 \text{ nm}$.

Energy-dispersive spectroscopy (EDS) was applied for the evaluation of the chemical composition of the samples using a TESCAN MIRA 3 Scanning Electron Microscope equipped with a Thermo Scientific EDS system in the WIGNER Research Center

for Physics. As shown by EDS data the chemical composition of the crystals corresponds to that of $\text{Cd}_2\text{P}_2\text{S}_6$ with the accuracy of the applied technique.

Silver paste, graphite, and vacuum-deposited gold were used as electrodes. All types of electrically conductive layers gave the same dielectric constant and loss tangent.

3. EXPERIMENTAL EQUIPMENT

Measurements of temperature dependences were carried out using an automated computer-controlled system¹⁵ in an immersion-type cryostat¹⁶ based on Measurement Computing USB-TEMP-AI data acquisition device and Linear Programmable DC Power Supply OWON ODP3033, which allows us to change the heating and cooling rate in the range of 0.001 K/min to 1 K/min. As a temperature sensor, the PT100/1509A platinum thermistor of TDI Ltd. company (England) was applied. The temperature measurement resolution was 0.001 K with an absolute accuracy of $\pm 2.9 \text{ K}$ at 73 K and 0.27 K at 373 K. To measure the dielectric constant, an LCR GW Insteek LCR-819 meter with a frequency range of 12 Hz – 100 kHz was chosen.

It should also be noted that when investigating thin layered hexatiohypodiphosphates, due to the small thickness of the samples (sometimes fractions of a micron), the measured field strength must be chosen with particular care. Standard instruments typically provide an output voltage of units of volts, which creates a measured field strength of units of kilovolts per centimeter (with a sample thickness of 1 μm). Taking into account the possible ionic conductivity (as in the case of $\text{CuInP}_2\text{S}(\text{Se})_6$), such fields can lead to changes in the properties of samples under the influence of the measured field (up to their destruction), and at least to a significant nonlinearity of the parameters under study. Such nonlinearity was observed in the case of $\text{Cd}_2\text{P}_2\text{S}_6$ crystals. As seen in Fig. 3, both components of the dielectric constant depend significantly on the measurement field strength. Taking this into account, all measurements were performed at the minimum voltage applied to the sample (in our case, 50 mV).

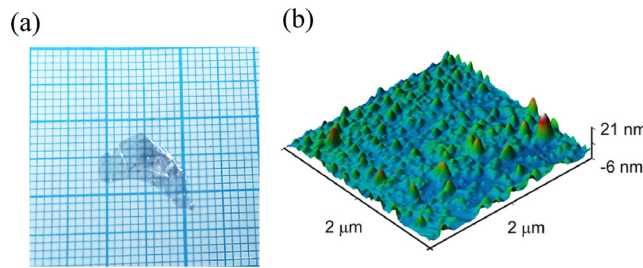


FIG. 2. Photograph of one of the investigated $\text{Cd}_2\text{P}_2\text{S}_6$ crystals (a), and a section of its surface (b), obtained with AFM.

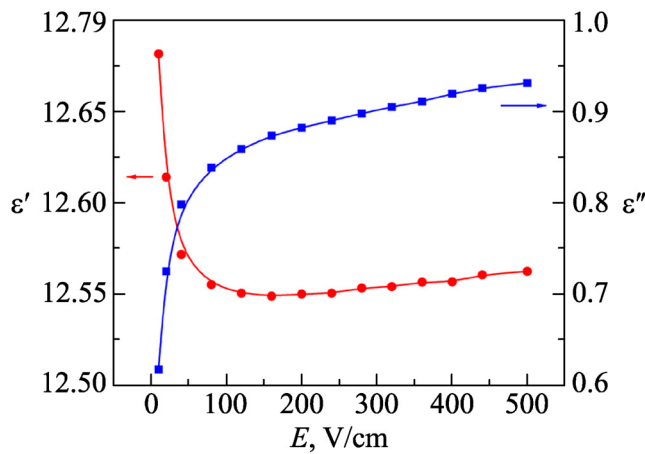


FIG. 3. Dependence of the complex permittivity components on the measurement field intensity for $\text{Cd}_2\text{P}_2\text{S}_6$ crystals at a frequency of 10 kHz.

4. EXPERIMENTAL RESULTS

We used $\text{Cd}_2\text{P}_2\text{S}_6$ samples with an area of 5×5 or 8×3 mm and a thickness of 10–15 μm for the experiments. Before use, the samples were examined using an optical microscope for the absence of cracks or interlayer holes. Gold electrodes were applied to the surface of crystals by vacuum deposition. To confirm the obtained results, two cycles of measurements were carried out using four different crystals from two process batches. Before each measurement, the samples were “annealed” at 400 K for 3 h. This was done to reduce the influence of “natural” intercalation of crystals by water or atmospheric components. Based on our previous studies, this process can effectively eliminate the prehistory of the samples and standardize them for equal experimental conditions. The temperature change rate for all experiments was 0.1 K per

minute. It should be taken into account that due to the use of an immersion-type cryostat our measurements take place in an atmosphere of nitrogen vapor.

We will consider the behavior of crystals from high temperatures (> 320 K) towards low temperatures (< 100 K).

4.1. High-temperature region

Despite the large width of the band gap of $\text{Cd}_2\text{P}_2\text{S}_6$ crystals, they are wide bandgap semiconductors, which is manifested in the high-temperature phase, where semiconductor behavior of both the real and imaginary parts of the dielectric constant is observed. This appears in the activation character of the temperature dependence of the parameters (increase in conductivity with increasing temperature, and consequently in the growth of the $\epsilon^*(T)$ components). With repeated cycles of temperature changes, i.e., changes in the heating to cooling mode, $\epsilon^*(T)$ increases [Figs. 4(a) and 4(b)].

It is difficult to carry out dc measurements in these samples due to their high resistance. Therefore, we measured the dielectric constant and losses at different frequencies, in the range of 100 Hz–100 kHz. In principle, our measuring system allows us to carry out measurements starting from 12 Hz, but the accuracy of the used measuring device decreases, which is manifested in a strong scatter of the obtained data, so they are not shown in Fig. 5.

The dependences obtained in cooling mode (blue points) and heating mode (red points) are presented in Figs. 5(a) and 5(b). We can observe that with decreasing frequency dielectric losses increase, especially in the high-temperature region, which is due to the growth of conductivity. This contribution leads to the growth of the real part of dielectric permittivity with decreasing frequency.

As experience shows, the anomalous behavior of $\epsilon(T)$ when modifying the direction or rate of temperature change (as demonstrated in Fig. 4) is characteristic of almost all materials of the $\text{Me}_2\text{P}_2\text{S}_6$ class, which most likely indicates a large role of the disequilibrium of the electronic subsystem on the temperature dependence of the electrophysical parameters of these crystals, and once

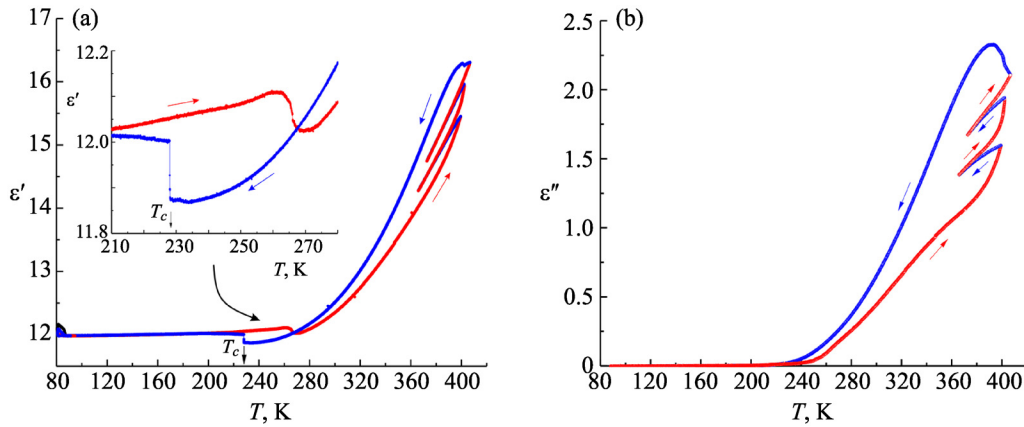


FIG. 4. Temperature dependences of the real part of the dielectric constant of $\text{Cd}_2\text{P}_2\text{S}_6$ crystals obtained in the heating and cooling regime measured at a frequency of 10 kHz. The inset shows an enlarged area of the phase transition region (a). Hysteresis of the imaginary part of the complex permittivity at temperature cycling in the region of 390 K (b).

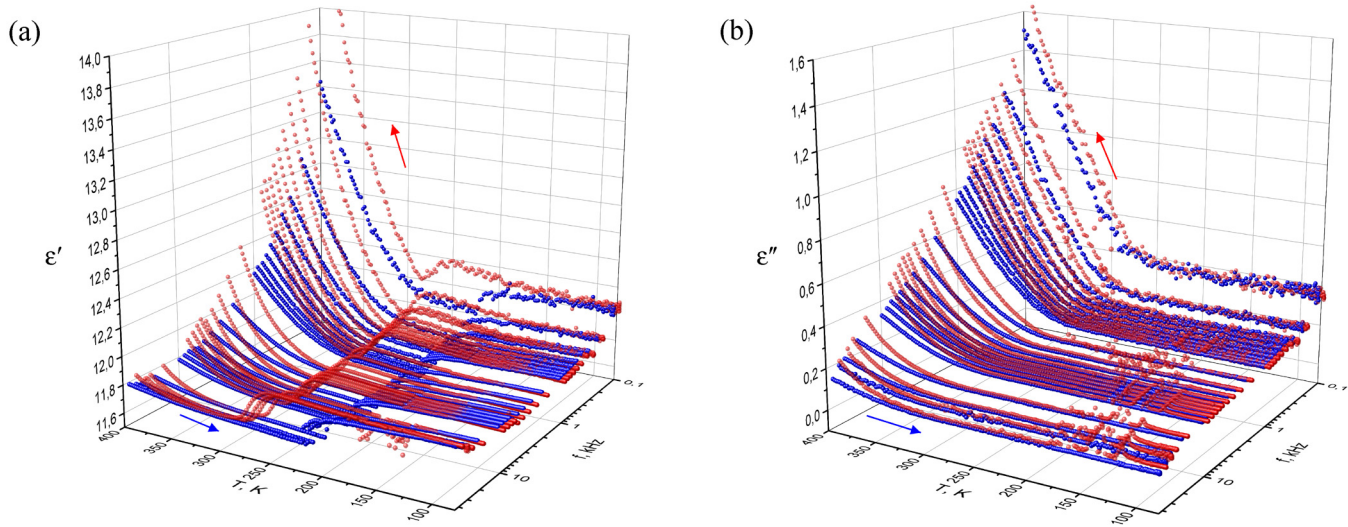


FIG. 5. Temperature dependences of the real $\epsilon'(T)$ (a) and imaginary $\epsilon''(T)$ (b) parts of the dielectric constant ϵ^* obtained at different frequencies, measured in the cooling and heating modes.

again confirms the need for measurements under quasi-stationary conditions.

However, $\text{Cd}_2\text{P}_2\text{S}_6$ crystals have a special behavior at high temperatures (Fig. 6). When the temperature stabilizes at 430 K, the dielectric constant and losses start to increase. In 10–12 h, this process never reaches saturation. The nonlinear behavior of the time dependence (deviation of ϵ' up and ϵ'' down) is most likely caused by a small temperature deviation during stabilization (seen in Fig. 6(a), in the form of a step on the vertical line). Earlier studies on $\text{Sn}_2\text{P}_2\text{S}_6$ and CuInP_2S_6 crystals did not reveal anything similar.

In the case of CuInP_2S_6 crystals, temperature stabilization in the vicinity of 370 K or higher does not lead to changes in the dielectric constant component with time.

In the case of $\text{Sn}_2\text{P}_2\text{S}_6$ crystals, the situation is slightly more complicated. This is due to the fact that, depending on the growth technology, $\text{Sn}_2\text{P}_2\text{S}_6$ crystals can have both high resistivity (obtained from the melt) and low resistivity (obtained from the gas phase). The difference in conductivity can be more than three orders of magnitude.

In high resistivity $\text{Sn}_2\text{P}_2\text{S}_6$ crystals, as we can see in Figs. 7(a) and 7(b) curve 1, stabilization of temperature in the paraelectric phase (at 378 K) does not lead to any observable changes in dielectric permittivity with time. This is due to the fact that this structure is highly defective, and the charge carriers are actively captured by defects in the structure so that their resistance is much higher than in gas-transport crystals, in which the concentration of defects is much smaller.

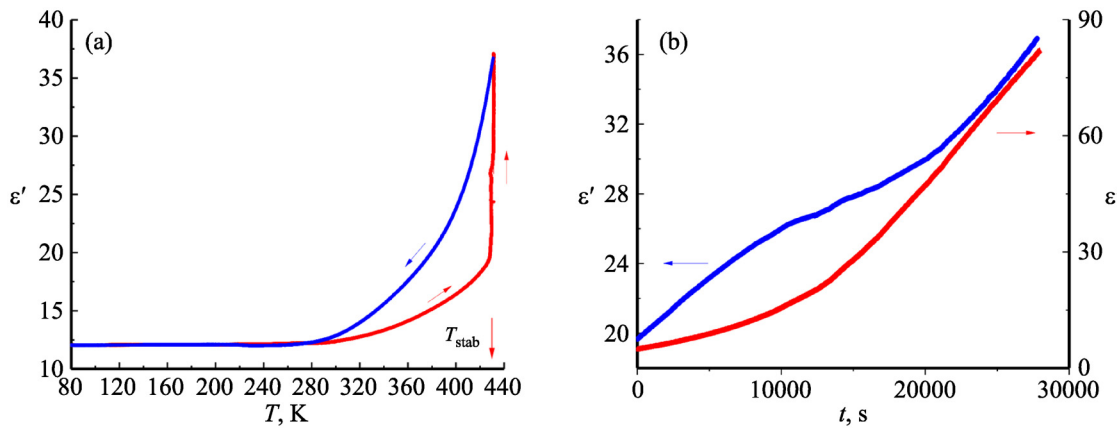


FIG. 6. Dielectric permittivity relaxation during temperature stabilization at 430 K for $\text{Cd}_2\text{P}_2\text{S}_6$ crystals at a frequency of 10 kHz.

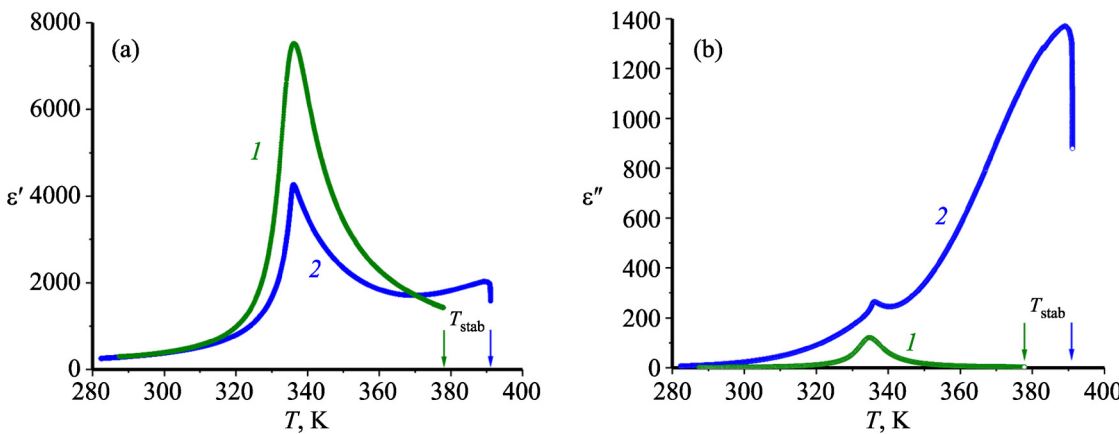


FIG. 7. The relaxation of the real ϵ' (a) and imaginary ϵ'' (b) parts of the dielectric constant ϵ^* of high-resistivity (1) and low-resistivity (2) $\text{Sn}_2\text{P}_2\text{S}_6$ crystals at 377 and 391 K. The measurements were taken after heating the crystals at a frequency of 10 kHz.

As shown in Ref. 17, the main charge carriers in $\text{Sn}_2\text{P}_2\text{S}_6$ crystals in both paraelectric and ferroelectric phases are holes. With increasing temperature, the concentration of both the main charge carriers and thermally activated electrons increases, which partially compensates for each other. However, the rate of increase in the concentration of electrons with increasing temperature is higher than that of holes. If the temperature change is stopped, the system enters an equilibrium state, electrons are trapped on traps in the forbidden zone (which, as was shown in Ref. 18, are due to small deviations of chemical composition from stoichiometry), which leads to a redistribution with time of the ratio of the concentration of electrons and holes, which is manifested in the decrease with time of conductivity and dielectric losses. As a result, we observe a decrease in both the real and imaginary components of the complex dielectric constant with time [Figs. 7(a) and 7(b) curve 2] at temperature stabilization at 392 K.

Given that the band gap width of CuInP₂S₆ crystals is 2.85 eV, and for $\text{Sn}_2\text{P}_2\text{S}_6$ crystals order 2.5 eV, it should be expected that in these materials temperature activation of conductivity will be manifested much stronger than in wide-band gap $\text{Cd}_2\text{P}_2\text{S}_6$ crystals. However, in practice, we see opposite behavior.

4.2. Phase transition region

The temperature dependences of the dielectric constant [Figs. 4(a) and 5(a)] clearly show a jump-like change in $\epsilon'(T)$ at 228 K in the cooling mode and 265 K in the heating mode. This behavior and the existence of a large temperature hysteresis confirm the first-order phase transition in $\text{Cd}_2\text{P}_2\text{S}_6$ crystals. In our opinion, this explains the discrepancy in the phase transition temperatures reported in Refs. 10 and 11. Most likely, the X-ray diffraction measurements in Ref. 10 were performed in the heating mode, and in Ref. 11 in the cooling mode.

Hysteresis of the phase transition temperature (its non-conformity in heating and cooling modes) is characteristic of first-order phase transitions since the system can be both “overcooled”

and “overheated”. For this purpose, as a rule, it is necessary to decrease the rate of temperature change. However, as always, there are exceptions.¹⁹ Therefore, a small variation in the phase transition temperature of $\text{Cd}_2\text{P}_2\text{S}_6$ crystals in different works is always present, and to account for it, it is necessary to specify the rate of temperature change and the mode of the experiment (it was performed in the heating or cooling mode).

4.3. Low temperature region

In the low-temperature region, in the range of 80–90 K, we can also observe a characteristic hysteresis behavior of dielectric

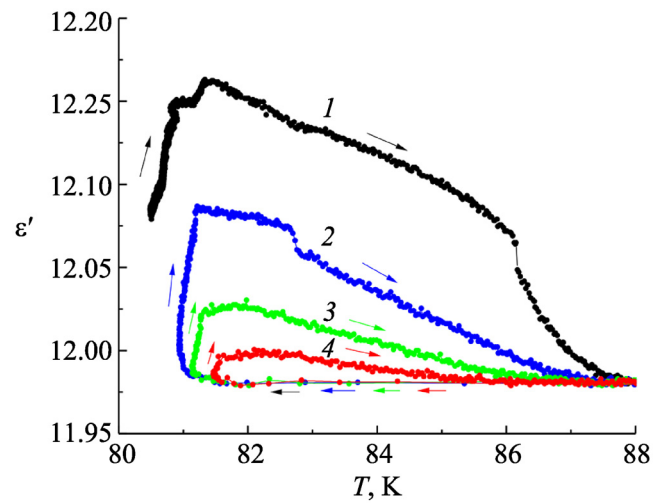


FIG. 8. Temperature dependences of the dielectric constant of $\text{Cd}_2\text{P}_2\text{S}_6$ crystals in the low-temperature region at cycling T . The numbers indicate the cycle number. All graphs were obtained at a measurement field frequency of 10 kHz.

permittivity during temperature cycling. Although this phenomenon has a very small amplitude (only 10% of the epsilon value), it is quite noticeable and is repeated on different samples. What is interesting, as we can see in Fig. 8, with each new temperature cycle the amplitude of the phenomenon decreases, and after the 4th, and 5th cycles the hysteresis disappears altogether. Two variants have been proposed to explain this behavior.

According to the first of them, there may be microcracks in the crystal, which, when the temperature changes due to thermal expansion, may lead to a change in the equivalent thickness of the sample. For layered crystals, growth defects in the form of microcracks or layer overlap disorders are often observed. To eliminate such effects, as described at the beginning of this paper, the excess defective layers of the samples were chipped off, to obtain a perfectly plane-parallel crystal with a high-quality surface layer. In addition, the samples were examined for micro defects using an optical microscope before electrode application. Although defects smaller than the resolution of the microscope could remain undetected, it is unlikely that they could make changes at the level of 10% dielectric permittivity. In addition, such defects should have manifested themselves in the region of higher temperatures, but we did not observe anything of that kind. Plus, if this phenomenon is caused by microcracks, repeated temperature cycling, on the contrary, should increase the hysteresis amplitude, since microcracks should grow (increase in size), and not heal. Therefore, our second assumption is more logical.

According to the second assumption, the presence of dielectric permittivity hysteresis at such low temperatures could be due to the intercalation of unknown gases or fluids into the interlayer space. In such a case, thermocycling behaves as a kind of pump, which, due to changes in the sample dimensions (including the interlayer distance), seems to push this intercalating substance out of the sample. This explains the decrease in the amplitude of the effect with each new cycle. When the intercalating substance completely leaves the sample, the hysteresis disappears. The question remains open as to why this phenomenon is observed only in the specified, limited temperature interval. But to get an answer to this question, further research will be required.

5. CONCLUSIONS

Based on the obtained results, we can conclude that in layered $\text{Cd}_2\text{P}_2\text{S}_6$ crystals in the temperature range of 80–400 K, three regions with hysteresis behavior of the dielectric permittivity are observed.

In the high-temperature region, the discrepancy between the temperature dependence of the ϵ^* during heating and cooling is due to the increase in conductivity, which is observed even when the temperature stabilizes.

A jump-like change in dielectric constant is found at 228 K in the cooling mode and 265 K in the heating mode, which is due to the first-order phase transition in these crystals.

At low temperatures, in the range of 80–90 K, there is also a hysteresis of the temperature dependence of the dielectric constant, the amplitude of which decreases with each cycle, and after the 4th–5th cycles, it disappears altogether. This behavior is most logically explained by the influence of the intercalating substance, which leaves the interlayer space during thermal cycling. However, further research is needed to explain this phenomenon.

ACKNOWLEDGMENTS

This work was funded in part by the HORIZON Project ID: 101131229 “2D Piezo” and the Ministry of Education and Science of Ukraine under project PH/41-2024 (0124U004302), focusing on “Layered ferroics MM’P2S(Se)6 with unique functional properties for nanoscale heterostructures.”

REFERENCES

- ¹X. Yang, Y. Luo, J. Li, H. Wang, Y. Song, J. Li, and Z. Guo, *Adv. Functional Mater.* **32**, 18 (2024).
- ²M. Labate, P. J. S. Foot, H. O’Malley, L. Miozzo, A. Papagni, L. Silvestri, P. Spearman, and S. Tavazzi, *J. Phys. Chem. C* **112**, 20149 (2008).
- ³M. G. Sendeku, K. Harrath, F. T. Dajan, B. Wu, S. Hussain, N. Gao *et al.*, *Nat. Commun.* **15**, 5174 (2024).
- ⁴Z. Cheng, M. G. Sendeku, and Q. Liu, *Nanotechnology* **31**, 135405 (2020).
- ⁵X. Yu and W. Ren, *Nat. Commun.* **14**, 5174 (2023).
- ⁶X. Qian, L. Chen, L. Yin, Z. Liu, S. Pei *et al.*, *Science* **370**, 596 (2020).
- ⁷P. Valencia, J. Manzur, A. M. García, V. Paredes-García, R. Cardoso-Gil *et al.*, *J. Chil. Chem. Soc.* **58**, 4 (2013).
- ⁸I. Lagadic, P. G. Lacroix, and R. Clément, *Chem. Mater.* **9**, 9 (1997).
- ⁹Z. Peng, Z. Cheng, S. Ke, Y. Xiao, Z. Ye, Z. Wang *et al.*, *Adv. Func. Mater.* **33**, 2211269 (2023).
- ¹⁰E. Lifshitz, A. H. Francis, and R. Clarke, *Solid State Commun.* **45**, 3 (1983).
- ¹¹F. Boucher, M. Evain, and R. Brec, *Acta Crystallographica. Section B* **51**, 952 (1995).
- ¹²V. Zhukov, F. Boucher, P. Alemany, M. Evain, and S. Alvarez, *Inorganic Chem.* **34**, 5 (1995).
- ¹³D. Yang, P. Westreich, and R. F. Frindt, *J. Solid State Chem.* **166**, 421 (2002).
- ¹⁴R. Nitsche and P. Wild, *Mater. Res. Bull.* **5**, 6 (1970).
- ¹⁵H. Bán, D. Gal, V. Gerasimov, A. Haysak, and A. Molnar, IDAACS 2021 The 11th IEEE International Conference on Intelligent Data Acquisition and Advanced Computing Systems: Technology and Applications, September 22–25, Cracow, Poland, 156 (2021).
- ¹⁶A. A. Molnar, *Uzhhorod University Scientific Herald. Series Physics* **40**, 148 (2016).
- ¹⁷Yu. Vysochanskii, K. Glukhov, M. Maior, K. Fedyo, A. Kohutych, V. Betsa, I. Prits, and M. Gurzan, *Ferroelectrics* **418**, 124 (2011).
- ¹⁸H. Ban, D. Gal, A. Kohutych, and A. Molnar, *Fiz. Nizk. Temp.* **50**, 59 (2024) [*Low Temp. Phys.* **50**, 56 (2024)].
- ¹⁹K. Z. Rushchanskii, A. Molnar, R. Bilanych, R. Yevych, A. Kohutych, and Yu. M. Vysochanskii, *Phys. Rev. B* **93**, 1 (2016).